Chapter 1
Image and Signal Sensors for Computing and Machine Vision: Developments to Meet Future Needs

Ross D. Jansen-van Vuuren, Ali Shahnewaz, and Ajay K. Pandey

Acronyms

ADC	Analogue-to-digital convertor
ASIC	Application-specific integrated circuit
CCD	Charge-coupled device
CFA	Colour filter array
CIS	CMOS image sensors
CMOS	Complementary metal-oxide semiconductor
CQDs	Colloidal quantum dots
D/A	Donor–acceptor
D^*	Specific detectivity
EQE	External quantum efficiency
FET	Field-effect transistor
FIT	Frame interline transfer
FT	Frame transfer
FWHM	Full width at half maximum
ICP	Integrated colour pixel
IoTs	Internet of things
IR	Infrared
J_d	Dark current
J_{ph}	Photocurrent

R. D. Jansen-van Vuuren (✉)
Department of Chemistry, Queen's University, Kingston, ON, Canada
e-mail: rdjv@queensu.ca

A. Shahnewaz · A. K. Pandey
School of Electrical Engineering and Computer Science, Queensland University of Technology, Brisbane, QLD, Australia
e-mail: shahnewaz.ali@hdr.qut.edu.au; a2.pandey@qut.edu.au

O. Sergiyenko et al. (eds.), *Machine Vision and Navigation*,
https://doi.org/10.1007/978-3-030-22587-2_1

LDR	Linear dynamic range
MVS	Machine vision systems
NEP	Noise-equivalent power
OFET	Organic field-effect transistor
OHP	Organohalide perovskite
OLED	Organic light-emitting diode
OPD	Organic photodiode
OPT	Organic phototransistor
OSC	Organic semiconductor
PT	Phototransistor
RGB	Red green blue (referring to a colour filter system)
ROIC	Read-out integrated circuitry
TFD	Transverse field detector
ToF	Time of flight

1.1 Introduction

1.1.1 Image Sensing in Machine Vision Systems

Digital cameras offer many advantages over conventional photo technologies, including the elimination of film processing, the ease of editing and affordability. Evidence for their increasing popularity worldwide can be seen in the resultant consumer success. The market for image sensors has experienced major growth over recent years with the value predicted to reach USD 23.97 billion by 2023 [1, 2]. This increase is largely due to digital still and video cameras, but also includes the expansion of digital imaging to cellular phones, laptop and personal computers (e.g. Internet-based video conferencing), security and surveillance, and the automotive, medical and entertainment industries. Digital cameras are also used extensively for image capture in machine vision systems (MVS), which rely upon object recognition and image analysis/indexing to extract data which is then used to control a process or activity. The applications of MVS are broad and range from automated industrial applications such as inspection and quality evaluation of products [3–5] to robotic guidance and control [6], autonomous vehicles [7–9], precision viticulture [10], picking and sorting fruit and vegetables [11] and colorimetric sorting systems [12].

Conventional image sensors are generally considered to be sufficient for consumer digital photography but are limited when meeting the level of imaging required for MVS applications which demand accurate and rapid colour image capture [6, 13], often in scenes of uncontrolled lighting with a large dynamic light range [14]. Furthermore, given the conditions under which imaging in rapidly advanced applications (e.g. self-driving cars, military applications, robotics) occurs, research is underway to find ways to develop photodetection systems which have the requisite size, lightness, compatibility with flexible and miniaturized substrates

and durability, preferably with a reduced cost. In order to try and meet these requirements, modifications to the sensing systems can be made including the use of different photodetector materials and/or image processing technologies, changes to the design and arrangement of the colour separation systems, altering the image sensor architectures or the individual pixel sensor arrangements (typically passive or active) or integration of 'smart functions' onto the chips of image sensors.

This chapter seeks to review the limitations of current MVS and the research being carried out to address these. The focus is largely upon applications which depend on colour image capture for object recognition and image indexing. MVS depending on colour recognition need to satisfy a vastly more complex requirement since 'color images include not only the brightness but also the color information, such as hue and saturation' [15, 16]. From the literature, the default approaches to improving colour recognition in MVS involve either modifying the image processing algorithms (these could include colour segmentation techniques) [15, 17] or exerting more control over the environmental conditions under which colour sensing takes place [3, 7, 18]. A key objective of this chapter is to flesh out two proposed alternative approaches, namely changes that can be made to the *architecture* of the image sensor and the *photosensor material* within the image sensor.

1.1.2 Image Capture by Digital Cameras

Firstly, consider the general set of operations carried out by a camera in capturing an image using an image sensor. The basic operations carried out by all digital cameras, regardless of their specific function and application, are essentially the same and consist of five separate steps [19]. These include: (1) photon collection, usually via a lens, which entails focusing the light before transmitting it through the optical system; (2) separation of the incoming photons by energy/wavelength (colour discrimination)—typically carried out using colour filter systems, for example Bayer colour filter array [20]; (3) (a) formation of photocurrent and (b) readout of the resultant signal (performed by the image sensor); (4) interpretation and processing of the data—now in digital form—in order to reproduce the colour image and (5) colour management and image compression processes as carried out by the microprocessor prior to data storage and export.

The image sensor plays the vital role of capturing the image, and the means by which this fundamentally occurs can be summarized in four steps [21]. (1) The absorption of photons by the photoactive material which constitutes the pixels, generating electron–hole pairs. (2) The electrons and holes are driven by means of an external electric field towards opposite electrodes, where they are extracted and give rise to the signal charge, which is collected and accumulated at each pixel. (3) The accumulated charge is then read out from each pixel in the two-dimensional array. Various means by which this occurs result in a range of different architectures giving rise to the range of image sensors on the current market, such as charge-coupled device (CCD) sensors, complementary metal-oxide semiconductor

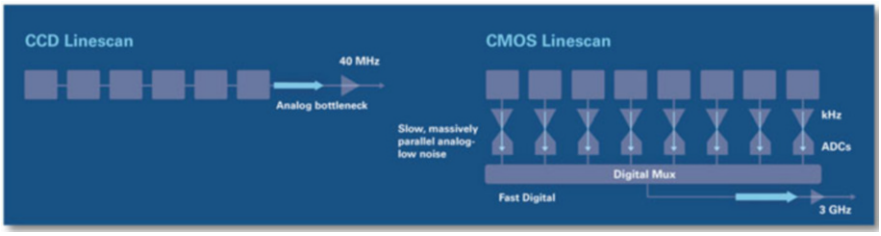

Fig. 1.1 General operation mechanism of a CCD versus that of a CMOS image sensor (image courtesy of [23])

(CMOS) sensors, MOS $x - y$ using addressed devices and frame transfer (FT) devices. (4) Finally, the charges are detected, which occurs in a manner that is essentially independent of the type of sensor. Although the different image sensor architectures commence at the same point, namely the transduction of photons to electrons, they differ in *how the charge is collected*. The most common image sensors have CCDs and CMOS architectures (Fig. 1.1). In general, CCDs, developed in the late 1960s, work by transporting the charge (generated through light absorption) across the chip to one corner of the photodiode array, before an analogue-to-digital convertor (ADC) transforms this into a digital signal, whereas in CMOS image sensors (CIS) (developed in the 1990s), photogenerated charge is collected at each pixel, before being amplified and transferred using traditional wiring (Fig. 1.1) [22].

Thus, CIS offer the following advantages over CCDs: 'ease of system integration, low power consumption, and freedom of device architecture' [22]. In addition, considering that machine vision systems require high speed with low noise during imaging, CMOS image sensors 'can be designed to have much lower noise than high speed CCDs', as shown in Fig. 1.1 [23]. There are multiple ways in which CIS can be configured—the two main approaches differ in the position of the light-receiving photodiodes: in front-illuminated CIS, the incoming light needs to pass through the colour filters and metal wiring before reaching the photodiode, whereas in back-illuminated CIS, the light reaches the photodiode more efficiently [22, 24]. Initially, due to their simple pixel layout, CCDs enabled more pixels per unit area and, therefore, higher pixel count and resolution. This was a major reason for their contribution towards the development and rise in popularity of digital still cameras [22, 25]. However, when CMOS image sensors made an appearance on the market, they rapidly gained popularity since the incorporation of 'in-pixel transistors' supported rapid image capture with low power consumption [22, 26]. The history of the development of CCDs and CMOS image sensors has been covered in detail elsewhere [27–29].

Although a major difference between the structure and operation of the various sensors lies in the method used to read out the signal produced by the photodetectors, it is the *type of photodetector material* and *means of colour recognition* within the camera that ultimately defines the quality of the image, since this has the largest influence over the spectral sensitivity and resolution of the sensor. There are several

approaches to capture colour images using conventional (broadband) photosensing materials. These can generally be classified into two major groupings which include (1) sensors which make use of an auxiliary structure that does not constitute the active layer of the pixel, such as a colour filter on top of the sensor cells, and (2) those in which the colour separation system is integrated within the imaging array (see Fig. 1.2). (1)(a) Although there are several arrangements of filters whose selection depends upon the application, a common system employs the Bayer filter [20], which consists of a mosaic of red (R), green (G) and blue (B) filters such that there are twice as many Gs as there are R and B to simulate the human visual system. (1)(b) The second method involves taking three sequential exposures, each with a different optical filter (RGB) mounted in a colour wheel [30], before combining the three separate images to form the final picture (Fig. 1.2b). (1)(c) The third approach involves the use of a beam-splitter, classically a trichroic prism assembly (Fig. 1.2c), which separates the light into its R, G and B components before these are focused onto three discrete image sensors ('3-CCD' or '3-CMOS'). Although considered somewhat superior in image quality and resolution, 3-CCD cameras are generally more expensive than single-sensors and the potential for miniaturization of cameras is somewhat limited [30]. (1)(d) An emerging technology called the integrated colour pixel (ICP) involves replacement of the colour filter array (CFA) with an array of metal strips in a specific pattern which enables colour separation during image capture. The patterned metal layers are placed within each pixel such that they control the transmission of light to the photodetector within the pixel [31].

In the second group, there are two approaches that can be taken. The first of these involves the direct absorption of red, green and blue lights at each location by stacking the colour pixels in a three-layer arrangement [32], as shown in Fig. 1.2. (2)(e). For example, this system is applied within the Foveon X3 direct image sensor [33, 34] and is similar in many respects to the layers of chemical emulsion comprising colour film. Foveon X3 image sensors have three layers of pixels, and each layer is embedded in silicon, taking advantage of the fact that red, green and blue lights penetrate silicon to different depths, therefore enabling an image sensor that captures full colour at every point in the captured image. Although stacked image sensors are able to increase the fill factor of the sensor surface area, as separate receptors are no longer required for each colour, the spectral sensitivity in these image sensing devices and the resultant colour reproducibility is insufficient to meet the demands of modern applications and cross-talk between layers presents a major device challenge [35, 36]. Finally, (2)(f) shows a method relying on the application of an electric field across the device, enabling the generation of carriers at varying but specific depths, subsequent to their collection [37, 38].

1.1.3 Performance Metrics of Image Sensor Photodiodes

Having covered the basic structure of modern image sensors and the various systems by which colour separation can be carried out, the figures of merit of photodetectors

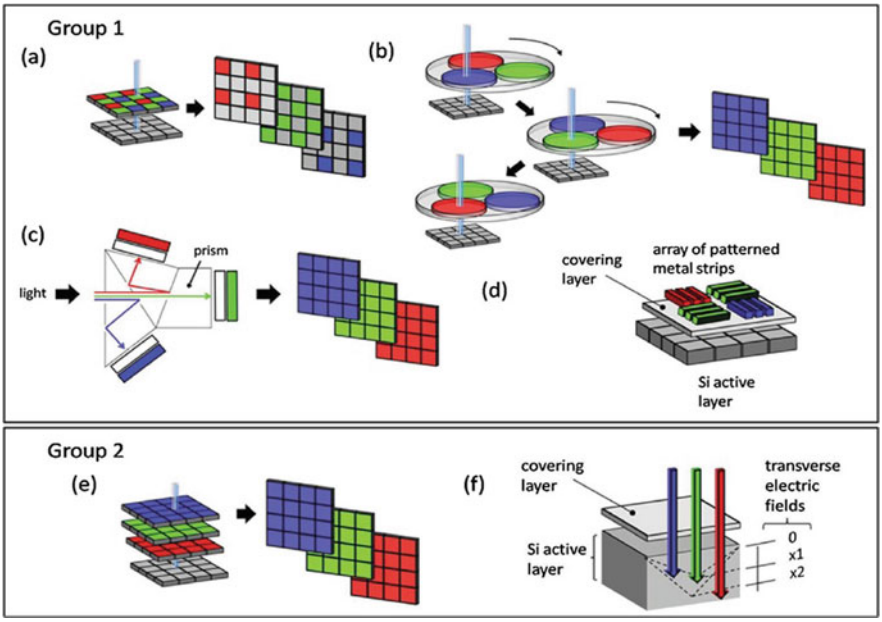

Fig. 1.2 The two main approaches for colour separation within broadband inorganic semiconductor photosensors. Group 1: (**a**) Bayer filter mosaic; (**b**) sequential triple exposure with R, G and B filters; (**c**) prism separation system and three sensor arrays (3MOS or 3CCD); (**d**) the Integrated Colour Pixel (ICP). Group 2—image sensors who achieve colour separation through an internal mechanism: (**e**) Foveon X3 image sensor; (**f**) Transverse Field Detector (TFD). Used with permission from Jansen-van Vuuren RD, Armin A, Pandey AK, Burn PL and Meredith PM (2016) Organic Photodiodes: The Future of Full Color Detection and Image Sensing. Advanced Materials, 28, 4766–4802. Copyright (2018) American Chemical Society. Taken from [39], Figure 2

(i.e. performance metrics) now need to be defined (Table 1.1), as these will be referred to in the text that follows. These metrics apply in general to the photodiodes within the image sensor, regardless of the material from which they are fabricated. Inorganic semiconductors are traditionally used, but these have limitations surrounding their use in MVS.

1.2 Limitations of Current Inorganic-Based Imaging Systems

Current image sensors in MVS are based on traditional silicon- or germanium-based technologies where silicon, Si (or germanium, Ge), is the material used as the photosensing material within the image sensor. III–V compounds such as InSb, GaN, AlN and InN are also used when a different bandgap is required. Si is the most commonly used semiconductor in optoelectronic devices due to its prevalence and the well-established technology enabling its integration within devices on large scales

Table 1.1 Performance metrics for photodetectors

Metric	Unit	Basic definition	Influenced by
Gain (G)	No unit	Number of photogenerated carriers circulating within the system divided by the number of incident photons	Active layer optical constants of material; charge transport; device optics
Photocurrent (J_{ph})	Amps (A)	Current flowing in a device as a result of illumination	Absorption coefficient of material; mobility, trapping and doping; electrode work functions
Dark current (J_d)	Amps (A) or nA/cm^2	Current flowing in a device without illumination	Mobility, trapping and doping; electrode work functions
Responsivity (R)	Watt/Amp (W A^{-1})	Ratio of photocurrent to the incident optical power (gives some idea of how efficiently the detector responds to an optical signal)	Absorption coefficient of material; mobility, trapping and doping; electrode work functions
External quantum efficiency (EQE)	%	Number of photogenerated carriers collected divided by the number of incident photons	Active layer optical constants of material; charge transport; device optics
Linear dynamic range (LDR)	Decibels (dB)	Range of incident light intensity to which the photodetector responds linearly	J_d, carrier mobilities, bimolecular recombination rate, device thickness
Noise-equivalent power (NEP)	Watt/Hertz (W Hz$^{-1/2}$)	Minimum light power detected—essentially a measure of the device sensitivity	Morphology; noise current, responsivity
Specific detectivity (D^*)	Jones (J)	The lower limit of light intensity detection (corresponds to NEP normalized to the device area and the electrical bandwidth of the noise measurement). D^* can be calculated as follows: $D^* = \frac{\sqrt{A}}{\text{NEP}}$, where A = the device area	Morphology; noise current, responsivity and device area
Spectral selectivity	Nanometres (nm)	Full width at half maximum (FWHM) of the spectral response	Properties of the photoactive chromophore (optical gap engineering); light matter interaction within the cavity (device)
Response speed/bandwidth (BW)	Hertz (Hz)	Speed of response, also known as the ‘operation frequency’ or ‘operation bandwidth’ of the signals detected	Charge carrier mobilities; charge trapping defects; range of light intensity and modulation frequency of the photo-response; thickness of material layer
Flexibility (mechanical strain)	Angle of tolerance (°)	Angle through which device can be bent without reducing J_{ph} reproducibly	Thickness, morphology

[40, 41]. Photodetectors used in current colour image-sensing applications are made from hydrogenated amorphous (*a*-Si:H) [42] or crystalline (c-Si) silicon [28]. This is typically deposited on top of the application-specific integrated circuit (ASIC), which is then responsible for the readout and processing of the photo signals. Photodiodes convert light into electrical signals by optical absorption resulting in the formation of electron–hole pairs which subsequently form separated charge carriers across a *p*-*n* junction. The charge separation occurs rapidly and without the need for an additional driving force, resulting in large charge mobilities (greater than 10^2 cm^2Vs^{-1}) [43] and nanosecond transient times, which has resulted in very high internal quantum efficiencies and sensitivities [44]. However, the significant problems with silicon (both amorphous and crystalline) with respect to photodetection for MVS are outlined as follows.

1.2.1 Weak Light Absorption

Si absorbs light relatively weakly over the visible spectrum [45], particularly in the blue region (400–460 nm) [32, 46]. While GaN detectors demonstrate superior UV light detection to Si, their practical use is still limited by cost and the need for complex architectures to achieve high detectivities [47]. In extremely low lighting, conventional PDs require low temperatures to reduce the J_d [48].

1.2.2 Low Dynamic Range

Firstly, image sensors fabricated with silicon photosensors are unable to cope with a high dynamic range (DR) of lighting. This can be experienced when trying to capture an image of a scene consisting of a very bright component as well as an object in complete shadow, resulting in the formation of images saturated either by bright white or dark black. This can be understood by considering the range in which the photocurrent generated by the photodiode is linearly dependent on the incident light power, with a tolerance of $\pm 1\%$. This range is called the linear dynamic range (LDR). Outside of the LDR, the device saturates completely at any incident light power level and the photodiode is said to be non-linear. The LDR depends on the wavelengths of light absorbed, the inherent properties of the photodiode (carrier mobility, device thickness and the noise current generated), the reverse bias applied and the resistance of the circuit in which the photodiode current is generated and collected. Silicon photodiodes have DRs of 100–120 dB [49], which corresponds to a J_{ph}/J_d of $\sim$6 orders of magnitude. Although this is discussed in more detail in subsequent sections, the highest value reported for organic photodetectors is 160 dB [50] and for metal halide perovskite photodetectors is 230 dB [51].

1.2.3 Incompatibility with Complicated Processing and Fabrication on Flexible, Miniaturized Devices

For many MVS applications, incompatibility of traditional inorganic semiconductors with read-out integrated circuitry (ROIC) presents a major obstacle to realizing compactness (whilst maintaining high detectivity and sensitivity) of light sensing devices [52]. Furthermore, since conventional inorganic semiconductors absorb a wide range of wavelengths, they require the use of colour filter arrays (and wavelength cut-off filters for colour sensing applications), thus complicating the design of such devices. Photodetectors consisting of c-Si, Si/Ge heterojunctions or III–V semiconductor alloys (e.g. InGaAs) are usually fabricated on rigid substrates, which precludes their applications in novel device concepts such as stretchable devices and bendable cameras [53]. The ability to conform to the various shapes of surfaces could simplify optical systems and enable the integration of photodiodes into miniaturized devices and ground robots [54].

1.2.4 Inability to Cope with Illuminant Variation

In general, MVS face a number of challenges when used in outdoor environments due to unpredictable and uncontrollable changes in the illumination [55–57]. The core reason for the inability of systems to cope under variable illuminance can be attributed to deficiencies in the photodetector portion of the image sensors. Silicon photodetectors are panchromatic and therefore unable to discriminate between photons having different wavelengths, relying on colour filters or depth-dependent absorption to form colour images [58], which results in images whose colour characteristics deviate from reality [7, 59, 60]. The need for colour filters additionally complicates the architecture and fabrication of imaging devices [61]. Humans possess an in-built capability called 'colour constancy' that enables the true perception of the colour of an object, regardless of illuminant, over a reasonable range of wavelengths [7]. Much research has focused on the development of image processing software able to compensate for this limitation by attempting to estimate the true colours of objects from the captured light through the use of algorithms. Indeed, there are other physical approaches to coping with illuminant variance, for example applying a digital filter to the output of the photosensor [62]; however, this text focuses on the use of a different image sensor material to achieve illuminant invariant image production.

1.2.5 Low Bandgap

Silicon also tends to have a smaller bandgap than required for visible detection, and therefore, the photodetectors require infrared (IR) filters in order to avoid unwanted IR sensitivity which contributes to excess noise [43, 63]. Group III–V compounds have different bandgaps, and therefore, wafers fabricated from these compounds offer variable options; however, these face most of the same issues already highlighted—lack of flexibility, complicated fabrication onto miniature or curved devices, etc.

1.2.6 Crosstalk

Despite the high mobilities and carrier lifetimes of silicon, this can also be regarded as disadvantageous as it causes crosstalk and distortion of the optical signals between neighbouring pixels, placing a high demand on the pixellation procedures, which are already delicately balanced between resolution and sensitivity [43, 64]. Pixel crosstalk can be attributed to leakage of photocurrent and/or the deflection and scattering of photons by adjacent pixels; both the effects (electrical and optical) contribute to reduction of the resolution of the colour and resolution of the final image [39].

1.3 Overcoming Limitations of Conventional Imaging Systems Using Alternative Photosensing Materials

The development of alternative semiconductor materials to fulfil some of the shortcomings presented by traditional inorganic semiconductors in photodetection forms a research field in its own right. The materials highlighted in the remainder of the chapter include semiconductors that can be processed under low-temperature conditions through ‘wet chemistry’ techniques, which include 3D printing, spray coating, spin coating, inkjet printing and doctor blading [52]. These approaches open up the possibility for large-area deposition and compatibility with substrates of different shapes and sizes and with flexible surfaces [53]. Furthermore, many of these alternative semiconductors have demonstrated similar and even superior performance metrics compared with their inorganic counterparts. The two major classes of materials that have been researched include (1) organic semiconductors (OSCs), and, more recently, (2) organohalide perovskites (OHPs). Although colloidal quantum dots (CQDs) have also been given research attention, these are yet to make meaningful gains in the production of image sensors. Therefore, CQDs will not be explored in this chapter. Organic semiconductors have been studied in greatest detail and so will be dealt with followed by OHPs.

1.3.1 Organic Photodetectors in Image Sensing

Organic semiconductors have already replaced inorganic materials in a range of applications available on the market, for example photovoltaic cells (NanoFlex Power Corporation, Infinitypv.com), light-emitting diodes LEDs (Sony OLED TVs, Panasonic OLED TVs, LG OLED TVs) and thin-film transistors (NeuDrive). The main reasons include the prospect of cheaper processing methods which involve solution-deposition or inkjet printing, the fact that they can be lightweight, thin and flexible, and the existence of a wide selection of organic materials which allows for tuning of the physical and optoelectronic properties. As a result, OPDs are in fact a 'disruptive technology' for MVS and large-area digital imagers as they enable 'lightweight, flexible, mechanically robust, and even conformable imagers' [65].

The first organic photodetector (OPD) was demonstrated in 1981 using dyes [66], before Yu and colleagues demonstrated a bulk heterojunction OPD with a sensitivity greater than that of UV-enhanced commercial Si-photodiodes in 1994 [67]. OPDs have since been developed with figures of metric that are comparable or even superior to traditional inorganic photodiodes [39, 49, 52, 68–70].

Compared with the three-dimensional networks of covalent bonds found in inorganic semiconductor structures such as silicon wafers, active films of organic semiconductors possess covalent intramolecular bonds but weak intermolecular van der Waals forces. This difference in the bonding systems results in the localization of the electronic wave function to individual molecules (instead of extending over the entire structure), which affects the separation of the electron–hole pairs in organic semiconductors, and their electronic bandwidth [71]. Optical excitation of organic semiconductors results in the formation of bound electron–hole pairs (called 'excitons') which can only be separated efficiently at a heterojunction of two materials with differing electron affinities. The energy difference between the electron affinities needs to be around 0.4–0.5 eV [72] to overcome the exciton-binding energy [73]. The separated holes and electrons then travel through the electron donor (D) and electron acceptor (A) materials, respectively, where they are extracted to the electrodes. For the process to work, the excitons need to diffuse to the D/A interface (the distance travelled by excitons is referred to as the exciton diffusion length and is typically 5–10 nm) [74]. During this process, there is a possibility of radiative or non-radiative recombination of the electron–hole pairs. Hence, exciton diffusion and separation must proceed more rapidly than the recombination processes. These steps, illustrated in Fig. 1.3c for the compounds shown in Fig. 1.3a, are fundamental to the conversion of light into electrical energy within excitonic (organic semiconductor-based) photodiodes.

Figure 1.3b illustrates the origin of J_d within photodetectors. Organic semiconductors may therefore play a part in reducing inter-pixel crosstalk since the excitonic movement from one pixel to the next is typically low and easily controlled.

Modifications to the chemical structures of the D or A compounds influence their packing in a film (morphology) and the electronic and optical energy levels, which in turn can lead to altered behaviour at the BHJ interfaces and different

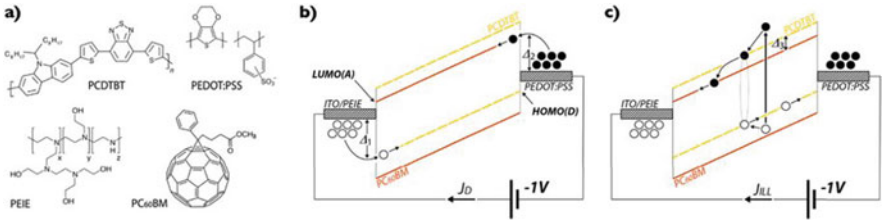

Fig. 1.3 (**a**) Chemical structures of PCDTBT (electron donor, D), PEDOT:PSS (top electrode), PEIE (ITO modifier) and PC60BM (electron acceptor, A); (**b**) Working principle of the photodetector in dark illustrating the origin of dark current and (**c**) under illumination showing the photovoltaic effect. Filled circles are electrons, empty circles represent holes (taken from [85], Fig 2, used through a Creative Commons Attribution 4.0 International License)

light sensitivities [75]. Thus, OPDs can be tuned, depending on the application requirements, enabling OPDs to overcome the low bandgap problem that is prevalent in inorganic semiconductors.

OPDs can be either 'broadband' or 'narrowband', depending on whether the semiconductor material absorbs light over a broad spectrum of wavelengths or a more narrow spectrum (typically absorbing one colour from the spectrum). Broadband OPDs can be incorporated into colour sensing systems in the same way as inorganic photosensors—using filters or stacking (or any of the other approaches shown in Fig. 1.2) [76, 77], with the same two major consequences previously described, namely (1) complicated device fabrication and (2) low colour accuracy under varying illuminant conditions. Deckman et al. (2018) report how a combination of a broadband OPD and broadband filters 'can successfully detect and reconstruct colors in the RGB system, with an average accuracy of 98.5%' [78]. Conversely, narrowband absorbing organic semiconductors enable the construction of filter-free photodetectors [79–81]. The use of four narrowband absorbers (each having an FWHM <100 nm) was found to be sufficient for achieving colour constancy for applications involving object recognition in MVS [82]. Other approaches to achieving narrowband and filter-free absorption involving the manipulation of the internal quantum efficiency of thick (μm) OPDs have been developed [50, 83, 84]. Thus, it is in this manner that OPDs are able to overcome a major limitation faced by traditional inorganic semiconductors—unable to cope with scenes of uncontrolled and variable illumination (e.g. in outdoor environments).

Although the concept of using organic materials as photodetectors is still relatively new, significant progress has been made, with organic semiconductors having superior photodetectivities, for example 1.03×10^{14} J at 735 nm under a positive +1 bias [86], higher linear dynamic responses over a wide spectral range, for example 160 dB for a broadband OPD [86] and 160 dB for a narrowband OPD [50], and similar J_ds (dark currents), for example 1.2×10^{-10} A/cm^2 [87], when compared with conventional inorganic photodiodes [88–92]. Thus, OPDs are able to overcome the weak light absorption and low dynamic range posed by traditional photodetectors.

Furthermore, the electro-optical properties of organic materials can be fine-tuned through simple modifications made to the chemical structure [93].

Image sensors have been fabricated with organic semiconductors as the photoactive layer [81, 94–98], demonstrating their applicability and feasibility in imaging and colour sensing. Samsung has reported the fabrication of image sensors with colour-selective OPDs [81, 99–101]. Panasonic has reportedly developed organic photosensing technologies, incorporating OPDs into an AK-SHB 810 model camera [102]. ISORG (based in Grenoble, France) has pioneered large-area OPDs and image sensors, collaborating with Plastic Logic in 2013 to co-develop the first OPD image sensor on plastic (Fig. 1.4) [103]. ISORG recently announced a substantial sum to be invested in developing value-added applications, 'primarily in personal electronic devices such as smartphones, wearables, tablets and laptops, biometrics for homeland security and medical imaging' [104].

Finally, OPDs have also been shown to demonstrate superior temperature stabilities compared with c-Si photodiodes [68]. This is a significant factor in the design of MVS for the applications in which the camera equipment is exposed to variable environmental conditions.

1.3.1.1 OPDs Beyond Photodetection

Current machine vision systems exploit CMOS technology for imaging, taking measurements, locating, identifying, inspecting or navigation. Emerging applications make use of CMOS image sensors in vision-based aerial imaging and navigation. In these latter applications, the camera technology has to be lightweight and low power-consuming to ensure economic viability and to be able to last over long flight durations. This would need development of new materials beyond discrete devices to full-fledged imaging systems. The previous section demonstrates that there is a strong potential for organic semiconductors in further simplifying the 2D layout of current camera technology. In this section, we present an outlook for organic and other family of advanced materials for their potential application

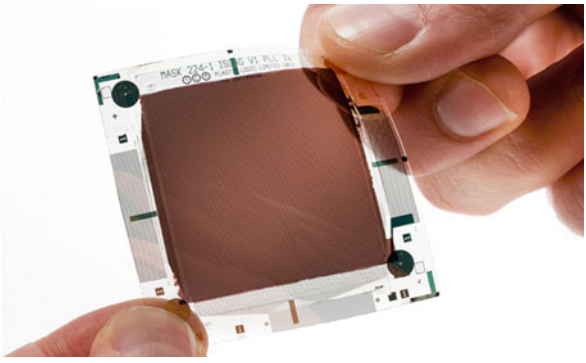

Fig. 1.4 Organic image sensor on a flexible organic thin-film transistor backplane (image used with permission, taken from [103])

in a number of new areas with a particular focus on how the research on this emerging technology should be aimed at integrating into advanced 3D imaging systems. The intrinsic advantages of OPD technology has not been realised, and features associated with spectral selectivity, tenability of multi-colour detection at relatively small form factors, mechanical flexibility and fabrication advantages are all poised to add intelligence at the pixel level. The ability to customise the sensor response without the need of complex fabrication protocols means OPD technology is suitable for combining shared intelligence at the hardware and software levels. These are some of the important attributes in achieving the next generation of smart, intelligent, light-weight and low-power demanding imaging systems for robotics and IoTs.

The cost of electronics has significantly reduced by integration of the emitter and receiver systems in integrated circuits. The ability to print light emitting diodes and organic photodetectors side by side would further allow denser integration of light signals and their detection. The recent emergence of bi- and multifunctional performance of organic optoelectronic devices offers great promise in simplifying the fabrication and integration of emitter and receiver functions by reducing the need of complex interconnects that reduce the effective form factors [105–109].

Conventional vision technology projects 3D world information into a 2D plane with no depth information. There is a growing demand for robust imaging technologies that can extend 2D imaging to 3D view of the scene in real time [110, 111]. For example, a robot with 3D vision can do more than detect the orientation of an object—it can actually *recognize* the object. This allows for intelligent, real-time decision-making and can be used to add intelligence to robot to learn quickly and be aware of the environment it is placed in [112, 113]. Microsoft has filed a patent application for a single handheld device that can detect material properties such as reflectivity, true colour and other properties of surfaces in a real-world environment [114]. The device exploits known relationships between lighting conditions, surface normals, true colour and image intensity.

Depth information improves system reliability and efficiency, for example an autonomous vehicle needs to perceive the objects present in the 3D scene from its sensors in order to plan its motion safely. It is important to highlight that the current state of the art imaging technologies still lack the ability to deal with a number of factors such as objects that have low textures or objects that are soft and deformable. Lighting conditions play an important role in the ability to image a scene, and the ability to design detectors that are selective to only a part of spectrum has great potential in reducing the artefacts introduced by ambient lighting. In this regard, spectrum or colour-selective OPDs have huge potential in improving image capture with constrained (indoor) or unconstrained (outdoor) environments. Therefore, OPDs have desirable attributes that can meet the application-specific requirements for diverse imaging environments including autonomous systems, mining, medical, social, aerial and marine robotics.

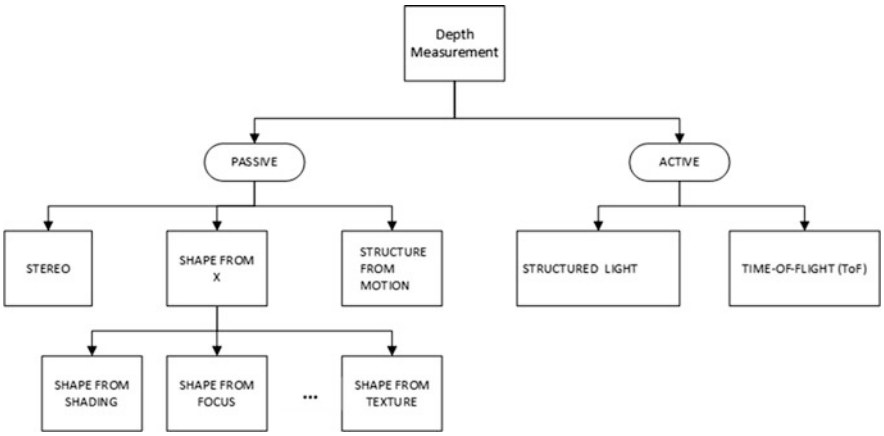

Fig. 1.5 Classification of depth measurement technology

Current depth sensor technologies can be classified into two main classes, as illustrated in Fig. 1.5. Passive estimation technology relies on machine learning algorithms and mathematical approaches which are used to extrapolate depth information from 2D image or images. The other class is active depth estimation technology, which relies on sensor technology or depth sensing devices to estimate distance. One aim of this section is to provide a path for OPDs and associated technologies to design devices that can measure or estimate depth using either a passive or an active approach.

Both passive and active depth measurement technology can provide depth perceptions of a scene. Active measurement technology is principally limited to image array size, therefore produces low-resolution images. Passive imaging technology uses natural or ambient illumination to capture scene. Most of the passive image sensors are based on charge-coupled device (CCD) or complementary metal-oxide semiconductor (CMOS).

OPDs for Depth Measurement Using Stereo Vision

Human vision is the most sophisticated and powerful vision solution to observe the environment and extract location information. Akin to the human visual system, robotic stereo vision forms a reliable depth perception technique for successful navigation of robots in unknown and unstructured environments [115]. The stereo vision technique requires two cameras to observe a scene from different locations and in turn produces different image locations of the objects. The disparity and baseline of the system are used for distance estimation and three-dimensional (3D) reconstruction of the scene. The simplest way to gain depth using OPDs is to fabricate

a set of OPD array that are separated by a known distance called the 'baseline'. There are no stereo cameras based on OPDs yet, but these can be readily fabricated to infer depth from 2D images. Computer vision algorithms are used to reconstruct depth from single or multiple images. Single-view 3D reconstruction methodology uses only one image. On the other side, multi-view 3D construction considers two or more images to reconstruct depth information. When two images are used, the system is known as a binocular stereo vision system, and probably it is the most widely focused research area of computer vision.

Stereo matching is the core technique of the stereo vision. Stereo matching is the process that matches each pixel from reference image to target and perceives the depth of each pixel. An intensive comparison takes place to find the corresponding pixel on the target image. Pre-configuration and pre-processing always take place before the actual stereo matching. In the stereo vision system, the reference and the target camera capture same scene point at the same time with a slightly different viewpoint. Stereo vision algorithms are based on this hypothesis. Therefore, the term synchronization is always used to convey the sense that the image acquisition system captures the same scene point at the same time with no time lag. When the object is in motion, this precondition plays a pivotal role to reduce reconstruction noises.

Calibration is the process that reduces image distortions. Stereo rectification is a transformation process that aligned two images into the same plane, so that same horizontal line becomes parallel to both the camera centres. Depth is calculated by finding the disparity in a pair of images. Disparity refers to the distance between two corresponding points in the left and right images of a stereo pair. It is inversely proportional to the depth and vice versa. In a stereo vision system, the relationship between depth and disparity can be expressed by the following equation:

$$d = b * f/z \tag{1.1}$$

where b is the baseline, f is the focal length, z stands for depth and disparity is expressed by the letter d. The basic idea of the disparity calculation is to match each pixel from the left image to the right image. In some circumstances, it may happen that some of the parts of a scene may not be visible through one or two cameras. This part of a scene is sometimes referred as a missing part. When this match process ends up, the difference of the pixel position in right image with respect to left image is known as disparity. Depth is estimated from the disparity by using the geometric principle of triangulation.

OPDs for Active 3D Imaging

In addition to an imaging array of photodetectors, the active 3D imaging system consists of a light source known as a projector. The aim of the projector is to emit signals. Received reflected signals are analysed to construct the 3D structure of the surrounding environments. Most commonly emitted signals are from a laser light source, an ultrasound signal or near infrared light. Many terms are used to describe

3D active imaging technology such as rangefinder, range imaging and 3D scanner. Several methods are used to measure the distance, but probably the most practiced principles are time of flight, triangulation and phase shift. This section provides a brief introduction of these three principles that OLED and OPD technology can use in inferring depth information from a scene. Dense depth map with less ambiguity and minimum depth error are the most reported advantages of active 3D imaging technology. However, the resolution of the depth map is limited. Miniaturized, high-resolution and low-power active depth sensors have a potential demand in various fields like medical and aerial robotics.

Among other systems, time-of-flight (ToF) systems measure the distance from the scanner to surface points through the measure of the time employed by the radiation to reach the object and come back to the scanner. This technique is very similar to the mobility measurement in organic semiconductors but albeit used here for imaging the real-world objects using a set of OPD arrays.

In this section, we focus on the time-of-flight (ToF) principle for OPDs. The basic idea of the active sensing technology is to emit photons as signal. When a compatible OLED projector emits the signal, then the clocking system inside the OPD-based imaging system can be set to start counting. This approach is known as direct ToF. If the object exists within the range of the imaging system, then it reflects a potential amount of signal to the camera. When the OPD receiver receives this signal, it then computes round trip time and from the basic principle of the light or electromagnetic source, the distance of the object from the camera can be estimated, using the following relationship:

$$d = \delta T * \text{light} \tag{1.2}$$

Within a defined range, ToF provides high-quality depth maps. The precise clock is the challenging part of this approach, and OPD systems would be limited by intrinsic mobility of organic materials used in the fabrication of such detectors. For example, when an object is placed very near to camera, for example in millimetre distance, it is challenging to design a clock that can measure a time gap in nanoseconds. OLEDs and OPDs based on high-mobility polymers with very high sensitivities should therefore be developed to meet the needs of active depth measurements. However, to keep aside the high-precise clock, the transmitter or projector could use a modulated signal. This approach is known as indirect time of flight. The transmitter could contain a signal emitter array of OLEDs to generate a modulated signal. Different kind of modulations is used such as sine, square, etc. The received signal is compared to the original signal. Different signal characteristics such as signal phase can be used to probe distance and resulting phase difference could be used to measure time and distance. It is a continuous process and more suitable for OPD and organic optoelectronics. The depth sensing technologies described here is equally applicable to organohalide perovskite or similar materials.

1.3.2 Metal Halide Perovskite (MHP)/Organohalide Perovskite (OHP) Photodetectors

MHPs and OHPs are compounds with a crystalline structure of the form ABX_3, where A and B represent cations of different sizes and X is an anion, typically a halide ion. In perovskites used to fabricate optoelectronic devices, A can represent an organic cation (e.g. methylammonium, $CH_3NH_3^+$) in the case of OHPs or an inorganic cation (e.g. Cs^+) in the case of MHPs, B is an inorganic cation (usually Pb^{2+} or Sn^{2+}), and X is a halide ion (I^-, Br^- or Cl^-). B and X together form an octahedron: $[BX_6]^{4-}$. A common example is methylammonium lead iodide, $CH_3NH_3PbI_3$: each unit cell of this compound consists of a central methylammonium ($CH_3NH_3^+$) in coordination with 12 anions of PbI_6 (occupying each corner), as shown in Fig. 1.6i [116]. Ion 'A' ($CH_3NH_3^+$) needs to be able to fit into the space between the eight octahedron, each connected to one another via 'corner-sharing' [117]. 'A' has a permanent electric dipole and is able to orient itself within the perovskite structure.

This ability to orient (and reorient) itself contributes to the high dielectric properties of perovskite materials, conferring upon the perovskites high mobilities and large diffusion lengths [118–120]. The good solution-processability and relatively low cost of perovskites, combined with their electric properties, give materials that are comparable to traditional crystalline Si and group III–V semiconductors [121]. Furthermore, solution-processable perovskites have absorption coefficients of $\approx 10^5$ cm^{-1} in the UV-visible section of the spectrum [122] and can therefore be

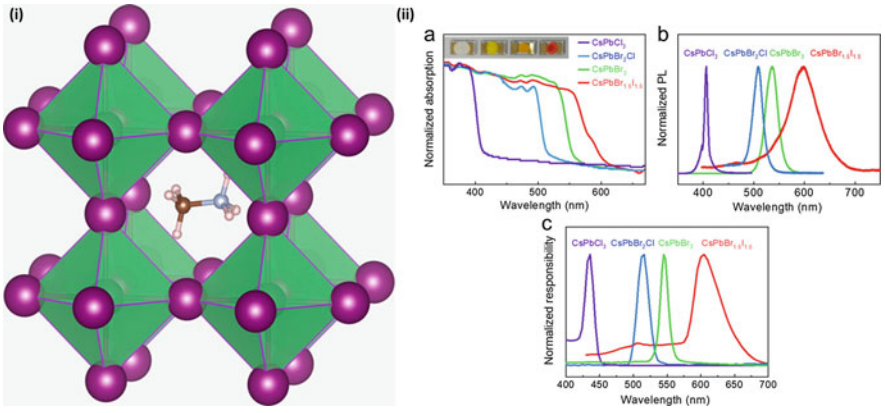

Fig. 1.6 (**i**) Methylammonium cation ($CH_3NH_3^+$) occupies the central 'A' site surrounded by 12 nearest-neighbour iodide ions in corner-sharing $[PbI_6]^{4-}$ octahedron (taken from [116], Fig 1; used through a Creative Commons Attribution 4.0 International License). (**ii**) Bandgap tuneability based on halide composition of the MHP: CsPbX demonstrated by (**a**) the tuneable absorption of the MHP within thin-film devices (inset: a photograph of the devices); (**b**) photoluminescence spectra of $CsPbX_3$ films and (**c**) normalized responsivity of $CsPbX_3$ photodetectors. Adapted with permission from Xue J, Zhu Z, Xu X, Wang S, Xu L, Zou Y, Song J, Zeng H and Chen Q (2018) Narrowband Perovskite Photodetector-Based Image Array for Potential Application in Artificial Vision. Nano Letters, 18(12):7628–7634. Copyright (2018) American Chemical Society

fabricated as thin films, with rapid response times [123]. Perovskites are also capable of high specific detectivities, and their bandgaps can be tuned based on the halide ratio (Fig. 1.6ii) [61], making them strong candidates for filter-free narrowband photodetectors capable of detection of light of specific wavelengths [123–127].

The first OHP photodiodes were only realized in 2015 [51, 128, 129]. In a similar fashion to OPDs, OHPs have been designed to be either broadband or narrowband absorbing, with the same implications regarding the use of colour filters as has been discussed for inorganic semiconductors and OPDs (see Fig. 1.2). Since then, intensive research has produced photodiodes with figures of merit comparable and superior to those of OPDs and inorganic photosensors. For example, a broadband OHP developed by Dou et al. (2014) demonstrated a J_d of 10^{-10} A/cm^2 (at 0 V) and a detectivity of 10^{14} Jones [128]. Lin et al. demonstrated narrowband, filter-free OHPs (absorbing light with wavelengths from 610 to 690 nm) with an LDR = 120 dB, $J_d = 5 \times 10^{-8}$ A/cm^2 (at −5 V) and a detectivity of 1.9×10^{11} Jones at 650 nm and under a −0.5 bias [130]. Hu et al. fabricated a flexible OHP using a 'vapour-solution' process with a very low J_d ($\sim 3 \times 10^{-5}$ A cm^{-2} at 1 V), an on/off ratio of 100 at 1 V, D^* greater than 10^{11} J and a linear response over 4 orders of magnitude incident power (at 680 nm and a bias of 1 V) [131].

OHPs have demonstrated the ability to switch between broadband and narrowband photodetection by changing between bottom and top illumination [118]. Furthermore, and in line with the scope of this article, OHPs have been integrated within image sensors and demonstrated reasonable performances [132–135]. For example, Wu and colleagues [133] fabricated a 10 × 10 flexible $CH_3NH_3PbI_{3-x}Cl_x$-based OHP array on a polyethylene terephthalate (PET) substrate as an image sensor demonstration. This flexible OHP image sensor demonstrated the following: (1) an on/off current ratio of 1.2×10^3 under illumination (38.3 mW/cm^2); (2) a detectivity (D^*) of up to 9.4×10^{11} Jones at a light intensity of 0.033 mW cm^{-1} (corresponding to a responsivity = 2.17 AW^{-1}) and (3) a stable electrical performance and no visible physical change under repeated bending (from 0° to 150°), with only a slight decrease observed for the light current (due to an increase in the resistance of the electrodes with bending).

Although OHPs are still relatively undeveloped (it has only been 4 years since the first OHP was conceived), large strides have been made, as shown by the performance metrics that have been achieved. In the same way that OPDs are able to overcome the limitations faced by inorganic photodetectors, OHPs offer tuneability and the opportunity to be fabricated on flexible substrates. More importantly, there is still much to be discovered in the area of organic photodetection using these materials.

1.4 Phototransistors

Until now, we have discussed two-terminal photodiode devices. A second type of architecture consists of three terminals—this is a phototransistor. The extra terminal enables the device to sense the level of light and modify the current flowing between

the emitter and the photosensor (and photon collector), based on the level of light received. Thus, phototransistors (PTs) or field-effect transistors (FETs) combine the photosensing function of a diode with a high gain, due to the electric field effects of transistors, making them more sensitive, capable of providing rapid output, and able to produce a higher current than PDs. PTs are therefore used widely in applications such as encoders, smart cards, active matrix displays and photodetection for artificial vision [136–138].

The organic PT (OPT) as a device platform is a natural extension to the more widely established organic field effect transistor (OFET) devices. First reported by Tsumura et al. [139] and subsequently developed by Horowitz et al. [140], OFETs are now used across different device platforms, from developing the basic understanding of electronic properties of organic semiconductors to chemical and bio-electronic sensors [141]. Figure 1.7a shows the typical layout of an OPT [105]. Figure 1.7b shows typical optical absorption spectra of the materials when fabricated as thin-film devices, demonstrating, in this case, how the absorption profiles evolve with a change in the proportion of donor and acceptor in the semiconductor blend.

In the operation of OPTs/OFETs, the saturation drain current ($I_{d,sat}$), which refers to the maximum current carried by the drain of the OPT when the gate source = 0, is given by the Horowitz equation [141]:

$$I_{d,sat} = \frac{W}{2L} C_i \mu_{FE} \left(V_g - V_t\right)^2, \tag{1.3}$$

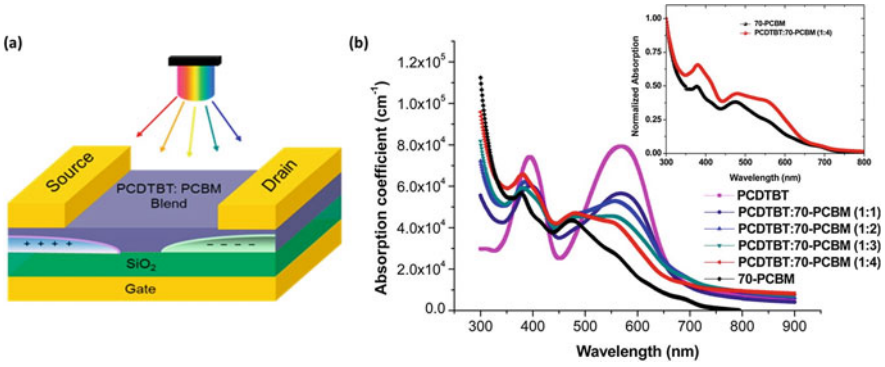

Fig. 1.7 (**a**) Device architecture of a typical OPT, in this case, with the light-absorbing layer consisting of poly[*N*-9′-heptadecanyl-2,7-carbazole-alt-5,5-(4′,7′-di-2-thienyl-2′,1′,3′-benzothiadiazole)] (PCDTBT) blended with [6,6]-phenyl C_{61} butyric acid methyl ester (PCBM). (**b**) Absorption spectra of the neat polymer PCDTBT, 70-PCBM and PCDTBT/70-PCBM blends (i.e. thin films) in 1:1–1:4 ratios (by weight) on glass substrates (inset shows the absorption profile of the 1:4 blend compared with that of a neat 70-PCBM thin film on glass). Adapted with permission from Pandey AK, Aljada M, Pivrikas A, Velusamy M, Burn PL, Meredith P and Namdas EB (2014) Dynamics of Charge Generation and Transport in Polymer-Fullerene Blends Elucidated Using a PhotoFET Architecture. ACS Photonics, 1(2):114–120, ref. [105]. Copyright (2014) American Chemical Society

where W is the width of the channel, L the length of the channel, C_i the capacitance per unit area of the gate dielectric, μ_{FE} the field-effect mobility, V_g the gate voltage and V_t the so-called threshold voltage.

The photocurrent generated in the presence of light is calculated by taking the difference of I_d under illumination and I_d in the dark. The responsivity of OPTs can be estimated by taking the photocurrent density (J_{ph}) in either the *p*- or *n*-channel mode of OPTs, using the following equation [105]:

$$J_{ph} = \frac{1}{s}\int_{\lambda=300\text{ nm}}^{\lambda=700\text{ nm}} \varphi(\lambda)\cdot \text{EQE}(\lambda)\, d\lambda \tag{1.4}$$

where s is the active surface area of the photoFET channel, φ is the photon-flux from light source, EQE is the external quantum efficiency of either the *p*- or the *n*-channel operation of the OPT and λ is the absorption onset and cut off wavelengths of the photosensing material (or composition).

Evidence of significant photosensing in an OPT platform was first reported by Narayan and Kumar in 2001 [142]. Then, a major boost in the widespread adoption of OPTs came from the demonstration of ambipolar operation of solution-processed OFETs by Meijer et al. [143]. Since then, research interest in combining the photosensing ability of OFETs with their operation has grown significantly, and it has emerged as a new class of organic optoelectronic device in its own right. Like OPDs, OPTs usually require a D-A network for efficient photosensing, and these different components can be fabricated by standard spin coating, inkjet printing or vacuum sublimation processes (described in previous sections). Lombardo and Dodabalapur evaluated the non-geminate recombination rate in P3HT:PCBM photovoltaic blends using an ambipolar OFET geometry [144]. The optical gap and transport properties of the main absorber usually defines the photosensing efficiency of OPTs. Pandey et al. demonstrated that some of the most efficient compositions of polymer:fullerene blends benefit from the light responsive and good charge transporting ability of fullerenes by operating OPTs in *p*- and *n*-channel modes [105]. In OPTs, the surface states at the organic–dielectric interface play an important role with this interface property, determining the performance of OFETs and therefore the efficiency of photosensing in OPTs [105, 145]. Furthermore, the high photoconductive gain coupled with 'sublinear responsivity to irradiance' of OPTs enables a wider LDR than for photodiode-based image sensors [146, 147], which would be of clear benefit to machine and robotic vision systems.

Variation to the photosensing layer by the use of organic–inorganic hybrid layer is seen as yet another extension of OPTs; for example this could include OHP PTs or hybrid organic–halide perovskite PTs (hybrid OHP PTs) [148, 149].

Baeg et al. provide a concise overview of OPTs [150]. A more comprehensive review on the diversity of solution-processed materials for photosensing applications in OPDs as well as OPTs is presented by Pelayo et al. [52] and Gasparini et al. [98]. An impressive photosensing performance under UV light exposure with high gain was demonstrated using vacuum-sublimed thin films of small molecules (copper phthalocyanine and para-sexiphenyl) in OPTs by Qian et al. [151]. Li et al. reported

high photoresponsivity (R) values of 320 A/W over a broad range of lighting spectrum for $CH_3NH_3PbI_3$-based OPH PTs [148].

OPTs have been integrated within image sensors and have demonstrated themselves fully capable of overcoming some of the limitations of conventional inorganic-based image sensors. For example, Pierre et al. developed a solution-processed OPT on a flexible substrate able to achieve a dynamic range of 103 dB for a video capture (30 frames/s) [146]. Milvich et al. designed and tested the performance of an array of 16 OPTs based on dinaphtho[2,3-b:2′,3′-f]thieno[3,2-b]thiophene covering an area of 2×4 cm^2 on a flexible PEN substrate [152].

The scope for OPTs in image sensors and MVS is expected to grow, and it will be interesting to see photosensing and switching functions further refined towards real-world applications.

1.5 Conclusions and Outlook

Current MVS have been recognized as having severe limitations when it comes to the demands of modern-day applications involving machine vision and robotics. These include weak light absorption over the visible range, low dynamic range, existence of crosstalk, an inability to cope with illuminant variation and incompatibility with complicated processing and fabrication on flexible, miniaturized devices. Such limitations could be overcome using alternative photoactive materials fabricated on the ROIC of the image sensor.

We have presented an outlook for further development of OPD systems for digital imaging, colour constancy and depth measurements. The soft, conformal and up-scaling of OPDs allow unparalleled possibilities of designed imaging systems that are not only low power-consuming and light-weight but highly intelligent in selective sensing over a range of applications.

While OHPs are still in the early stages of understanding and development, much has been accomplished already, and their potential for transforming the landscape of machine vision and artificial vision in robotic systems will surely dawn in the near future.

Knowledge translation [153, 154] is key to realizing the potential of both OPDs and OHPs in commercial machine and robotic vision systems. Furthermore, a more cross-disciplinary approach needs to be implemented to harness the potential of OPDs and OHPs in MVS; at the moment, the field lacks chemists and material scientists with a strong knowledge of image sensing, machine vision and future market trends. Likewise, camera experts are largely ignorant of the advances made in developing alternative semiconductor materials able to replace Si or InGaAs. The authors hope that this chapter helps to bridge this gap and initiate conversations between chemists, physicists, material scientists and mechatronic engineers.

References

1. ResearchandMarkets.com. (2018). *Global image sensors market analysis, growth, trends & forecast 2018-2023*. Retrieved February 21, 2019, from https://www.businesswire.com/news/home/20180530005711/en/Global-Image-Sensors-Market-Analysis-Growth-Trends
2. IC insights. (2018). *CMOS image sensor sales stay on record-breaking pace*. Retrieved February 21, 2019, from http://www.icinsights.com/data/articles/documents/1065.pdf
3. Cubero, S., Aleixos, N., Moltó, E., Gómez-Sanchis, J., & Blasco, J. (2011). Advances in machine vision applications for automatic inspection and quality evaluation of fruits and vegetables. *Food and Bioprocess Technology, 4*(4), 487–504.
4. Patel, K., Kar, A., Jha, S., & Khan, M. (2011). Machine vision system: A tool for quality inspection of food and agricultural products. *Journal of Food Science Technology, 49*(2), 1–19.
5. Kaur, H., Sawhney, B. K., & Jawandha, S. K. (2018). Evaluation of plum fruit maturity by image processing techniques. *Journal of Food Science and Technology, 55*(8), 3008–3015.
6. Sridharan, M., & Stone, P. (2009). Color learning and illumination invariance on mobile robots: A survey. *Robotics and Autonomous Systems, 57*, 629–644.
7. Marchant, J. A., Tillett, N. D., & Onyango, C. M. (2004). Dealing with color changes caused by natural illumination in outdoor machine vision. *Cybernetics and Systems: An International Journal, 35*(1), 19–33.
8. Buluswar, S. D., & Draper, B. A. (1998). Color machine vision for autonomous vehicles. *Engineering Applications of Artificial Intelligence, 11*, 245–256.
9. Maddern, W., Stewart, A. D., McManus, C., Upcroft, B., Churchill, W., & Newman, P. (2014). Illumination invariant imaging: Applications in robust vision-based localisation, mapping and classification for autonomous vehicles. In *Proceedings of the Visual Place Recognition in Changing Environments Workshop, IEEE International Conference on Robotics and Automation*.
10. Fernández, R., Montes, H., Salinas, C., Sarria, J., & Armada, M. (2013). Combination of RGB and multispectral imagery for discrimination of cabernet sauvignon grapevine elements. *Sensors (Basel, Switzerland), 13*(6), 7838–7859.
11. Bloss, R. (2013). Robots use machine vision and other smart sensors to aid innovative picking, packing and palletizing. *Industrial Robot: An International Journal, 40*(6), 525–529.
12. Oestreich, J. M., Tolley, W. K., & Rice, D. A. (1995). The development of a color sensor system to measure mineral compositions. *Minerals Engineering, 8*(1/2), 31–39.
13. Schmittmann, O., & Lammers, P. S. (2017). A true-color sensor and suitable evaluation algorithm for plant recognition. *Sensors, 17*(8), 1823.
14. Yamada, K., Nakano, T., & Yamamoto, S. (1998). A vision sensor having an expanded dynamic range for autonomous vehicles. *IEEE Transactions on Vehicular Technology, 47*(1), 332–341.
15. Xiong, N. N., Yang, S., Kangye, Y., Changhoon, L., & Chunxue, W. (2018). Color sensors and their applications based on real-time color image segmentation for cyber physical systems. *EURASIP Journal on Image and Video Processing, 2018*, 23.
16. Pathare, P. B., Opara, U. L., & Al-Said, F. A. (2013). Colour measurement and analysis in fresh and processed foods: A review. *Food and Bioprocess Technology, 6*(1), 36–60.
17. Ratnasingam, S., & Collins, S. (2008). An algorithm to determine the chromaticity under non-uniform illuminant. In *ICISP 2008: Image and signal processing* (pp. 244–253).
18. Logvinenko, A. D., Funt, B., Mirzaei, H., & Tokunaga, R. (2015). Rethinking colour constancy. *PLoS One, 10*(9), e0135029.
19. Lukac, R., Plataniotis, K. N., & Hatzinakos, D. (2005). Color image zooming on the Bayer pattern. *IEEE Transactions on Circuits and Systems for Video Technology, 15*(11), 1475–1492.
20. Bayer, B. E. (1975). *Color imaging array*. U.S. Patent No. 3,971,065.
21. Nakamura, J. (2006). Basics of image sensors. In *Image sensors and signal processing for digital still cameras* (pp. 55–61). Boca Raton, FL: Taylor & Francis.

22. Suzuki, T. (2010). Challenges of image-sensor development. In *2010 IEEE International Solid-State Circuits Conference—(ISSCC)* (pp. 28–30).
23. *Teledyne Dalsa, CCD vs CMOS*. Retrieved March 30, 2019, from https://www.teledynedalsa.com/en/learn/knowledge-center/ccd-vs-cmos/
24. Lahav, A., Fenigstein, A., & Strum, A. (2014). Backside illuminated (BSI) complementary metal-oxide-semiconductor (CMOS) image sensors. In *High performance silicon imaging fundamentals and applications of CMOS and CCD sensors* (pp. 98–123).
25. Nomoto, T., Oike, Y., & Wakabayashi, H. (2016). Accelerating the sensing world through imaging evolution. In *2016 Symposium on VLSI Circuits Digest of Technical Papers* (pp. 1–4).
26. Fossum, E. R. (1997). CMOS image sensors: Electronic camera-on-a-chip. In *IEEE Proceedings of International Electron Devices Meeting*.
27. Fossum, E. R., & Hondongwa, D. B. (2014). A review of the pinned photodiode for CCD and CMOS image sensors. *IEEE Journal of the Electron Devices Society, 2*(3), 33–43.
28. Bigas, M., Cabruja, E., Forest, J., & Salvi, J. (2006). Review of CMOS image sensors. *Microelectronics Journal, 37*(5), 433–451.
29. Lesser, M. (2014). Charge coupled device (CCD) image sensors. In *High performance silicon imaging: Fundamentals and applications of CMOS and CCD sensors* (pp. 78–97).
30. Hamilton, G., Brown, N., Oseroff, V., Huey, B., Segraves, R., Sudar, D., Kumler, J., Albertson, D., & Pinkel, D. (2006). A large field CCD system for quantitative imaging of microarrays. *Nucleic Acids Research, 34*(8), e58, 1–e58,14.
31. Catrysse, P., & Wandell, B. A. (2003). Integrated color pixels in 0.18-μm complementary metal oxide semiconductor technology. *Journal of the Optical Society of America A, 20*(12), 2293–2306.
32. Knipp, D., Herzog, P. G., & Stiebig, H. (2002). Stacked amorphous silicon color sensors. *IEEE Transactions on Electron Devices, 49*(1), 170–176.
33. Hubel, P. M. (2005). Foveon technology and the changing landscape of digital cameras. In *13th IS&T Color Imaging Conf., Scottsdale, AZ, USA* (pp. 314–317).
34. Lyon, R., & Hubel, P. M. (2002). Eyeing the camera: Into the next century. In *IS&T/TSID 10th Color Imaging Conference Proceedings Scottsdale, AZ* (p. 349).
35. Blockstein, L., & Yadid-Pecht, O. (2010). Crosstalk quantification, analysis, and trends in CMOS image sensors. *Applied Optics, 49*(24), 4483–4488.
36. Anzagira, L., & Fossum, E. R. (2015). Color filter array patterns for small-pixel image sensors with substantial cross talk. *Journal of the Optical Society of America A, 32*(1), 28–34.
37. Langfelder, G., Longoni, A., & Zaraga, F. (2009). Further developments on a novel color sensitive CMOS detector. In *Proceedings Volume 7356, Optical Sensors 2009; 73562A*.
38. Longoni, A., Zaraga, F., Langfelder, G., & Bombelli, L. (2008). The transverse field detector (TFD): A novel color-sensitive CMOS device. *IEEE Electron Device Letters, 29*(12), 1306–1308.
39. Jansen-van Vuuren, R. D., Armin, A., Pandey, A. K., Burn, P. L., & Meredith, P. M. (2016). Organic photodiodes: The future of full color detection and image sensing. *Advanced Materials, 28*, 4766–4802.
40. Moloney, A. M., Wall, L., Mathewson, A., Healy, G., & Jackson, J. C. (2006). Novel black silicon PIN photodiodes. In *Proceedings Volume 6119, Semiconductor Photodetectors III; 61190B*.
41. Tut, T., & Dan, Y. (2014). Silicon photodetectors integrated with vertical silicon nitride waveguides as image sensor pixels: Fabrication and characterization. *Journal of Vacuum Science & Technology B, 32*, 031201.
42. Theil, J. A., Snyder, R., Hula, D., Lindahl, K., Haddad, H., & Roland, J. (2002). a-Si:H photodiode technology for advanced CMOS active pixel sensor imagers. *Journal of Non-Crystalline Solids, 299–302*, 1234–1239.
43. Konstantatos, G., & Sargent, E. H. (2010). Nanostructured materials for photon detection. *Nature Nanotechnology, 5*, 391–400.

44. Konstantatos, G., & Sargent, E. H. (2009). Solution-processed quantum dot photodetectors. *Proceedings of the IEEE, 97*(10), 1666–1683.
45. Goetzberger, A., & Hebling, C. (2000). Photovoltaic materials, past, present, future. *Solar Energy Materials and Solar Cells, 62*(1–2), 1–19.
46. Lule, T., Benthien, S., Keller, H., Mutze, F., Rieve, P., Seibel, K., Sommer, M., & Bohm, M. (2000). Sensitivity of CMOS based imagers and scaling perspectives. *IEEE Transactions on Electron Devices, 47*(11), 2110–2122.
47. Liu, L., Yang, C., Patanè, A., Yu, Z., Yan, F., Wang, K., Lu, H., Liab, J., & Zhao, L. (2017). High-detectivity ultraviolet photodetectors based on laterally mesoporous GaN. *Nanoscale, 9*, 8142–8148.
48. Haddadi, A., Dehzangi, A., Adhikary, S., Chevallier, R., & Razeghi, M. (2017). Background–limited long wavelength infrared InAs/InAs1- xSbx type-II superlattice-based photodetectors operating at 110 K. *Applied Physics Letters Materials, 5*, 035502.
49. Gong, X., Tong, M., Xia, Y., Cai, W., Moon, J. S., Cao, Y., Yu, G., Shieh, C.-L., Nilsson, B., & Heeger, A. J. (2009). High-detectivity polymer photodetectors with spectral response from 300 nm to 1450 nm. *Science, 325*(5948), 1665–1667.
50. Armin, A., Jansen-van Vuuren, R. D., Kopidakis, N., Burn, P. L., & Meredith, P. (2015). Narrowband light detection via internal quantum efficiency manipulation of organic photodiodes. *Nature Communications, 6*, 6343.
51. Lin, Q., Armin, A., Lyons, D. M., Burn, P. L., & Meredith, P. (2015). Low noise, IR-blind organohalide perovskite photodiodes for visible light detection and imaging. *Advanced Materials, 27*(12), 2060–2064.
52. Pelayo de García de Arquer, F., Armin, A., Meredith, P., & Sargent, E. H. (2017). Solution-processed semiconductors for next-generation photodetectors. *Nature Reviews Materials, 2*(16100), 1–16.
53. Xie, C., & Yan, F. (2017). Flexible photodetectors based on novel functional materials. *Small, 13*(43), 1701822(1 of 36).
54. Ng, T. N., Wong, W. S., Lujan, R. A., & Street, R. A. (2009). Characterization of charge collection in photodiodes under mechanical strain: Comparison between organic bulk heterojunction and amorphous silicon. *Advanced Materials, 21*(18), 1855–1859.
55. Vasavi, V., Shaik, A. F., & Sunkara, P. C. K. (2018). Moving object classification under illumination changes using binary descriptors. In M. Rivas-Lopez, O. Sergiyenko, W. Flores-Fuentes, & J. C. Rodríguez-Quiñonez (Eds.), *Optoelectronics in machine vision-based theories and applications* (pp. 188–189). Hershey, PA: IGI Global.
56. Ji, W., Zhao, D., Cheng, F., Xu, B., Zhang, Y., & Wang, J. (2012). Automatic recognition vision system guided for apple harvesting robot. *Computers and Electrical Engineering, 38*(5), 1186–1195.
57. Son, J., Kim, S., & Sohn, K. (2015). A multi-vision sensor-based fast localization system with image matching for challenging outdoor environments. *Expert Systems with Applications, 42*(22), 8830–8839.
58. Antognazza, M. R., Musitelli, D., Perissinotto, S., & Lanzani, S. (2010). Spectrally selected photodiodes for colorimetric application. *Organic Electronics, 11*(3), 357–362.
59. Xiong, J., Liu, Z., Lin, R., Bu, R., He, Z., Yang, Z., & Liang, C. (2018). Green grape detection and picking-point calculation in a night-time natural environment using a charge-coupled device (CCD) vision sensor with artificial illumination. *Sensors, 18*(969), 1–17.
60. Ratnasingam, S., & McGinnity, T. M. (2012). Chromaticity space for illuminant invariant recognition. *IEEE Transactions on Image Processing, 21*(8), 3612–3623.
61. Xue, J., Zhu, Z., Xu, X., Wang, S., Xu, L., Zou, Y., Song, J., Zeng, H., & Chen, Q. (2018). Narrowband perovskite photodetector-based image array for potential application in artificial vision. *Nano Letters, 18*(12), 7628–7634.
62. Flores-Fuentes, W., Miranda-Vega, J. E., Rivas-López, M., Sergiyenko, O., Rodríguez-Quiñonez, J. C., & Lindner, L. (2018). Comparison between different types of sensors used in the real operational environment based on optical scanning system. *Sensors, 18*(1684), 1–15.

63. Guo, W., Rage, U. K., & Ninomiya, S. (2013). Illumination invariant segmentation of vegetation for time series wheat images based on decision tree model. *Computers and Electronics in Agriculture, 96*, 58–66.
64. Estribeau, M., & Magnan, P. (2005). CMOS pixels crosstalk mapping and its influence on measurements accuracy for space applications. In *Proceedings of SPIE, Volume 5978, Sensors, Systems, and Next-Generation Satellites IX; 597813*.
65. Natali, D., & Caironi, M. (2016). Organic photodetectors. In *Photodetectors, materials, devices and applications* (p. 233).
66. Kudo, K., & Moriizumi, T. (1981). Spectrum-controllable color sensors using organic dyes. *Applied Physics Letters, 39*, 609–611.
67. Yu, G., Pakbaz, K., & Heeger, A. J. (1994). Semiconducting polymer diodes: Large size, low cost photodetectors with excellent visible-ultraviolet sensitivity. *Applied Physics Letters, 64*, 3422–3424.
68. Biele, M., Benavides, C. M., Hürdler, J., Tedde, S. F., Brabec, C. J., & Schmidt, O. (2019). Spray-coated organic photodetectors and image sensors with silicon-like performance. *Advanced Materials Technologies, 4*(1), 1800158:1–6.
69. Yang, D., & Ma, D. (2019). Development of organic semiconductor photodetectors: From mechanism to applications. *Advanced Optical Materials, 7*(1), 1800522:1–23.
70. Cai, S. (2019). Materials and designs for wearable photodetectors. *Advanced Materials, Early View, 31*(18), 1808138.
71. Natali, D., & Sampietro, M. (2003). Detectors based on organic materials: Status and perspectives. *Nuclear Instruments and Methods in Physics Research Section A: Accelerators, Spectrometers, Detectors and Associated Equipment, 512*(1–2), 419–426.
72. Arkhipov, V. I., & Bässler, H. (2003). Exciton dissociation and charge photogeneration in pristine and doped conjugated polymers. *Physica Status Solidi A, 201*(6), 1152–1187.
73. Gregg, B. A. (2003). Excitonic solar cells. *Journal of Physical Chemistry B, 107*(20), 4688–4698.
74. Thompson, B. C., & Fréchet, J. M. J. (2007). Polymer–fullerene composite solar cells. *Angewandte Chemie International Edition, 47*(1), 58–77.
75. Rauch, T., Henseler, D., Schilinsky, P., Waldauf, C., Hauch, J., Brabec, C. J. (2004). Performance of bulk-heterojunction organic photodetectors. In *4th IEEE Conference on Nanotechnology*.
76. Yu, G., Wang, J., McElvain, J., & Heeger, A. J. (1999). Large-area, full-color image sensors made with semiconducting polymers. *Advanced Materials, 10*(17), 1431–1434.
77. Seo, H., Aihara, S., Watabe, T., Ohtake, H., Sakai, T., Kubota, M., Egami, N., Hiramatsu, T., Matsuda, T., & Furuta, M. (2011). A 128×96 pixel stack-type color image sensor: Stack of individual blue-, green-, and red-sensitive organic photoconductive films integrated with a ZnO thin film transistor readout circuit. *Japanese Journal of Applied Physics, 50*, 024103.
78. Deckman, I., Lechêne, P. B., Pierre, A., & Arias, A. C. (2018). All-printed full-color pixel organic photodiode array with a single active layer. *Organic Electronics, 56*, 139–145.
79. Jansen-van Vuuren, R. D., Pivrikas, A., Pandey, A. K., & Burn, P. L. (2013). Colour selective organic photodetectors utilizing ketocyanine-cored dendrimers. *Journal of Materials Chemistry C, 1*, 3532–3543.
80. Jansen-van Vuuren, R. D., Johnstone, K. D., Ratnasingam, S., Barcena, H., Deakin, P. C., Pandey, A. K., Burn, P. L., Collins, S., & Samuel, I. D. W. (2010). Determining the absorption tolerance of single chromophore photodiodes for machine vision. *Applied Physics Letters, 96*, 253303.
81. Han, M. G., Park, K.-B., Bulliard, X., Lee, G. H., Yun, S., Leem, D.-S., Heo, C.-J., Yagi, T., Sakurai, R., Ro, T., Lim, S.-J., Sul, S., Na, K., Ahn, J., Jin, Y. W., & Lee, S. (2016). Narrow-band organic photodiodes for high-resolution imaging. *Applied Materials and Interfaces, 8*(39), 26143–26151.
82. Ratnasingam, S., & Collins, S. (2010). Study of the photodetector characteristics of a camera for color constancy in natural scenes. *Journal of the Optical Society of America A, 27*(2), 286–294.

83. Yoon, S., Koh, C. W., Woo, H. Y., & Chung, D. S. (2018). Systematic optical design of constituting layers to realize high-performance red-selective thin-film organic photodiodes. *Advanced Optical Materials, 6*(4), 1701085.
84. Yazmaciyan, A., Meredith, P., & Armin, A. (2019). Cavity enhanced organic photodiodes with charge collection narrowing. *Advanced Optical Materials, Early View, 7*(8), 1801543.
85. Kielar, M., Dhez, O., Pecastaings, G., Curutchet, A., & Hirsh, L. (2016). Long-term stable organic photodetectors with ultra low dark currents for high detectivity applications. *Scientific Reports, 6*(39201), 1–11.
86. Nie, R., Deng, X., Feng, L., Hu, G., Wang, Y., Yu, G., & Xu, J. (2017). Highly sensitive and broadband organic photodetectors with fast speed gain and large linear dynamic range at low forward bias. *Small, 13*(24), 1603260.
87. Hu, L., Han, J., Qiao, W., Zhou, X., Wang, C., Ma, D., Li, Y., & Wang, Z. H. (2018). Side-chain engineering in naphthalenediimide-based n-type polymers for high-performance all-polymer photodetectors. *Polymer Chemistry, 9*(3), 327–334.
88. *Si image sensor S1336-18BK, Hamamatsu Photonics KK*. Retrieved February 28, 2019, from https://www.datasheets360.com/part/detail/s1336-18bk/1668072914334887650/
89. *InGaAs image sensor G10899-03K, Hamamatsu*. Retrieved February 28, 2019, from https://www.hamamatsu.com/us/en/product/type/G10899-03K/index.html
90. *Si (S6428-01) blue light absorbing image sensor, Hamamatsu*. Retrieved February 28, 2019, from https://www.hamamatsu.com/us/en/product/type/S6428-01/index.html
91. *Si (S6429-01) green light absorbing image sensor, Hamamatsu*. Retrieved February 28, 2019, from https://www.hamamatsu.com/us/en/product/type/S6429-01/index.html
92. *Si (S6430-01) red light absorbing image sensor, Hamamatsu*. Retrieved February 28, 2019, from https://www.hamamatsu.com/us/en/product/type/S6430-01/index.html
93. Jansen-van Vuuren, R. D., Deakin, P. C., Olsen, S., & Burn, P. L. (2014). Tuning the optoelectronic properties of cyanine and ketocyanine dyes by incorporation of 9,9-di-*n*-propylfluorenylindolenine. *Dyes and Pigments, 101*, 1–8.
94. Jahnel, M., Tomshcke, M., Fehse, K., Vogel, U., An, J. D., Park, H., & Im, C. (2015). Integration of near infrared and visible organic photodiodes on a complementary metal–oxide–semiconductor compatible backplane. *Thin Solid Films, 592*(Part A), 94–98.
95. Zalar, P., Matsuhisa, N., Suzuki, T., Enomoto, S., Koizumi, M., Yokota, T., Sekino, M., & Someya, T. (2018). A monolithically processed rectifying pixel for high-resolution organic imagers. *Advanced Electronic Materials, 4*(6), 1700601.
96. Swathi, K., & Narayan, K. S. (2016). Image pixel device using integrated organic electronic components. *Applied Physics Letters, 109*, 193302.
97. Baierl, D., Pancheri, L., Schmidt, M., Stoppa, D., Betta, G.-F. D., Scarpa, G., & Lugli, P. (2012). A hybrid CMOS-imager with a solution-processable polymer as photoactive layer. *Nature Communications, 3*, 1175.
98. Gasparini, N., Gregori, A., Salvador, M., Biele, M., Wadsworth, A., Tedde, S., Baran, D., McCulloch, I., & Brabec, C. J. (2018). Visible and near-infrared imaging with nonfullerene-based photodetectors. *Advanced Materials Technologies, 3*(7), 1800104.
99. Lim, S.-J., Leem, D.-S., Park, K.-B., Kim, K.-S., Sul, S., Na, K., Lee, G. H., Heo, C.-J., Lee, K.-H., Bulliard, X., Satoh, R.-I., Yagi, T., Ro, T., Im, D., Jung, J., Lee, M., Lee, T.-Y., Han, M. G., Jin, W. Y., & Lee, S. (2015). Organic-on-silicon complementary metal–oxide–semiconductor colour image sensors. *Scientific Reports, 5*, 7708.
100. Lee, K.-H., Leem, D.-S., Castrucci, J. S., Park, K.-B., Bulliard, X., Kim, K.-S., Jin, Y. W., Lee, S., Bender, T. P., & Park, S. Y. (2013). Green-sensitive organic photodetectors with high sensitivity and spectral selectivity using subphthalocyanine derivatives. *ACS Applied Materials and Interfaces, 5*(24), 13089–13095.
101. Leem, D.-S., Lim, S.-J., Bulliard, X., Lee, G. H., Lee, K.-H., Yun, S., Yagi, T., Satoh, R.-I., Park, K.-B., Choi, Y. S., Jin, Y. W., Lee, S. (2016). Recent developments in green light sensitive organic photodetectors for hybrid CMOS image sensor applications (conference presentation). In *SPIE Proceedings, 9944, Organic Sensors and Bioelectronics IX; 99440B*.

102. Panasonic Corporation. (2018). *Panasonic develops industry's first 8K high-resolution, high performance, global shutter technology using organic-photoconductive-film cmos image sensor*. Press Release. Retrieved February 28, 2019, from https://news.panasonic.com/global/press/data/2018/02/en180214-2/en180214-2.pdf
103. Editor. (2019). *The OSA direct newsletter. ISORG and plastic logic co-develop the world's first organic image sensor on plastic*. Retrieved February 28, 2019, from http://www.osadirect.com/news/article/980/isorg-and-plastic-logic-co-develop-the-worlds-first-organic-image-sensor-on-plastic/
104. Andrew Lloyd & Associates. (2018). *Isorg raises €24M to finance the ramp up of large-scale commercialization*. Retrieved February 28, 2019, from http://ala.com/isorg-raises-e24m-to-finance-the-ramp-up-of-large-scale-commercialization/
105. Pandey, A. K., Aljada, M., Pivrikas, A., Velusamy, M., Burn, P. L., Meredith, P., & Namdas, E. B. (2014). Dynamics of charge generation and transport in polymer-fullerene blends elucidated using a PhotoFET architecture. *ACS Photonics, 1*(2), 114–120.
106. Ullah, M., Yambem, S. D., Moore, E. G., Namdas, E. B., & Pandey, A. K. (2015). Singlet fission and triplet exciton dynamics in rubrene/fullerene heterojunctions: Implications for electroluminescence. *Advanced Electronic Materials, 1*(12), 1500229.
107. Pandey, A. K. (2015). Highly efficient spin-conversion effect leading to energy up-converted electroluminescence in singlet fission photovoltaics. *Scientific Reports, 5*, 7787.
108. Lee, W., Kobayashi, S., Nagase, M., Jimbo, Y., Saito, I., Inoue, Y., & Yambe, T. (2018). Nonthrombogenic, stretchable, active multielectrode array for electroanatomical mapping. *Science, 4*(10), eaau2426.
109. Rogers, J., Malliaras, G., & Someya, T. (2018). Biomedical devices go wild. *Science Advances, 4*(9), eaav1889.
110. Bock, R. D. (2018). Low-cost 3D security camera. In *Proceedings Volume 10643, Autonomous Systems: Sensors, Vehicles, Security, and the Internet of Everything; 106430E*.
111. Semeniutaa, O., Dransfeld, S., Martinsena, K., & Falkmanc, P. (2018). Towards increased intelligence and automatic improvement in industrial vision systems. In *11th CIRP Conference on Intelligent Computation in Manufacturing Engineering—CIRP ICME'17* (pp. 256–261).
112. Smith, L. N., Zhang, W., Hansen, M. F., Hales, I. J., & Smith, M. L. (2018). Innovative 3D and 2D machine vision methods for analysis of plants and crops in the field. *Computers in Industry, 97*, 122–131.
113. Haouchine, N., Kuang, W., Cotin, S., & Yip, M. (2018). Vision-based force feedback estimation for robot-assisted surgery using instrument-constrained biomechanical three-dimensional maps. *IEEE Robotics and Automation Letters, 3*(3), 2160–2165.
114. Hilliges, O., Weiss, H. M., Izadi, S., Kim, D., & Rother, C. C. E. (2018). *Using photometric stereo for 3D environment modeling*. US Patent Application US9857470B2.
115. Murray, D., & Little, J. J. (2000). Using real-time stereo vision for mobile robot navigation. *Autonomous Robots, 8*(161), 161–171.
116. Eames, C., Frost, J. M., Barnes, P. R. F., O'Regan, B. C., Walsh, A., & Islam, M. S. (2015). Ionic transport in hybrid lead iodide perovskite solar cells. *Nature Communications, 6*, 7497.
117. Saparov, B., & Mitzi, D. B. (2016). Organic–inorganic perovskites: Structural versatility for functional materials design. *Chemical Reviews, 116*(7), 4558–4596.
118. Saidaminov, M. I., Haque, M. A., Savoie, M., Abdelhady, A. L., Cho, N., Dursun, I., Buttner, U., Alarousu, E., Wu, T., & Bakr, O. M. (2016). Perovskite photodetectors operating in both narrowband and broadband regimes. *Advanced Materials, 28*(37), 8144–8149.
119. Xiao, Z. (2016). Thin-film semiconductor perspective of organometal trihalide perovskite materials for high-efficiency solar cells. *Materials Science and Engineering: R: Reports, 101*, 1–38.
120. Strainks, S. D., Eperon, G. E., Grancini, G., Menelaou, C., Alcocer, M. J. P., Leijtens, T., Herz, L. M., Petrozza, A., & Snaith, H. J. (2013). Electron-hole diffusion lengths exceeding 1 micrometer in an organometal trihalide perovskite absorber. *Science, 342*(6156), 341–344.

121. Brenner, T. M., Egger, D. A., Kronik, L., Hodes, G., & Cahen, D. (2016). Hybrid organic—Inorganic perovskites: Low-cost semiconductors with intriguing charge-transport properties. *Nature Reviews Materials, 1*, 15007.
122. Burschka, J., Pellet, N., Moon, S.-J., Humphry-Baker, R., Gao, P., Nazeeruddin, M. K., & Grätzel, M. (2013). Sequential deposition as a route to high-performance perovskite-sensitized solar cells. *Nature, 499*, 316–319.
123. Ahmadi, M., Wu, T., & Hu, B. (2017). A review on organic–inorganic halide perovskite photodetectors: Device engineering and fundamental physics. *Advanced Materials, 29*(41), 1605242.
124. Zhou, J., & Huang, J. (2017). Photodetectors based on organic–inorganic hybrid lead halide perovskites. *Advanced Materials, 5*(1), 1700256.
125. Wang, H., & Kim, D. H. (2017). Perovskite-based photodetectors: Materials and devices. *Chemistry Society Reviews, 46*, 5204–5236.
126. Wang, X., Li, M., Zhang, B., Wang, H., Zhao, Y., & Wang, B. (2018). Recent progress in organometal halide perovskite photodetectors. *Organic Electronics, 52*, 172–183.
127. Tian, W., Zhou, H., & Li, L. (2017). Hybrid organic–inorganic perovskite photodetectors. *Small, 13*(41), 1702107.
128. Dou, L., Yang, Y. M., You, J., Hong, Z., Chang, W.-H., Li, G., & Yang, Y. (2014). Solution-processed hybrid perovskite photodetectors with high detectivity. *Nature Communications, 5*, 5404.
129. Sutherland, B. R., Johnston, A. K., Ip, A. H., Xu, J., Adinolfi, V., Kanjanaboos, P., & Sargent, E. H. (2015). Sensitive, fast, and stable perovskite photodetectors exploiting interface engineering. *ACS Photonics, 2*(8), 1117–1123.
130. Lin, Q., Armin, A., Burn, P. L., & Meredith, P. (2015). Filterless narrowband visible photodetectors. *Nature Photonics, 9*, 687–694.
131. Hu, W., Huang, W., Yang, S., Wang, X., Jiang, Z., Zhu, X., Zhou, H., Liu, H., Zhang, Q., Zhuang, X., Yang, J., Kim, D. H., & Pan, A. (2017). High-performance flexible photodetectors based on high- quality perovskite thin films by a vapor–solution method. *Advanced Materials, 29*(43), 1703256.
132. Lee, W., Lee, J., Yun, H., Kim, J., Park, J., Choi, C., Kim, D. C., Seo, H., Lee, H., Yu, J. W., Lee, W. B., & Kim, D.-H. (2017). Perovskite thin films: High-resolution spin-on-patterning of perovskite thin films for a multiplexed image sensor array. *Advanced Materials, 29*(40), 1702902.
133. Wu, W., Wang, X., Han, X., Yang, Z., Gao, G., Zhang, Y., Hu, J., Tan, Y., Pan, A., & Pan, C. (2018). Flexible photodetector arrays based on patterned $CH_3NH_3PbI_{3-x}Cl_x$ perovskite film for real-time photosensing and imaging. *Advanced Materials, 31*(3), 1805913.
134. Lyashenko, D., Perez, A., & Zakhidov, A. (2016). High-resolution patterning of organohalide lead perovskite pixels for photodetectors using orthogonal photolithography. *Physica Status Solid A, 214*(1), 1600302.
135. Gu, L., Tavakoli, M. M., Zhang, D., Zhang, Q., Waleed, A., Xiao, Y., Tsui, K.-H., Lin, Y., Liao, L., Wang, J., & Fan, Z. (2016). 3D arrays of 1024-pixel image sensors based on lead halide perovskite nanowires. *Advanced Materials, 28*(44), 9713–9721.
136. Kim, M. S., Lee, G. J., Kim, H. M., & Song, Y. M. (2017). Parametric optimization of lateral NIPIN phototransistors for flexible image sensors. *Sensors, 17*(8), 1774:1–13.
137. Tomioka, K., Miyake, K., Misawa, K., Toyoda, K., Ishizaki, T., & Kimura, M. (2018). Photosensing circuit using thin-film transistors for retinal prosthesis. *Japanese Journal of Applied Physics, 57*, 1002B1.
138. Kimura, M., Miura, Y., Ogura, T., Ohno, S., Hachida, T., Nishizaki, Y., & Shima, T. (2010). Device characterization of p/i/n thin-film phototransistor for photosensor applications. *IEEE Electron Device Letters, 31*(9), 984–986.
139. Tsumura, A., Koezuka, H., & Ando, T. (1986). Macromolecular electronic device: Field-effect transistor with a polythiophene thin film. *Applied Physics Letters, 49*, 1210.
140. Horowitz, G., Fichou, D., Peng, X., Xu, Z., & Garnier, F. (1989). A field-effect transistor based on conjugated alpha-sexithienyl. *Solid State Communications, 72*(4), 381–384.

141. Horowitz, G. (2004). Organic thin film transistors: From theory to real devices. *Journal of Materials Research, 19*(7), 1946–1962.
142. Narayan, K. S., & Kumar, N. (2001). Light responsive polymer field-effect transistor. *Applied Physics Letters, 79*, 1891.
143. Meijer, E. J., Leeuw, D. M. D., Setayesh, S., Van Veenendaal, E., Huisman, B.-H., Blom, P. W. M., Hummelen, J. C., Scherf, U., & Klapwijk, T. M. (2003). Solution-processed ambipolar organic field-effect transistors and inverters. *Nature Materials, 2*, 678–682.
144. Ooi, Z.-E., Danielson, E., Liang, K., Lombardo, C., & Dodabalapur, A. (2014). Evaluating charge carrier mobility balance in organic bulk heterojunctions using lateral device structures. *Journal of Physical Chemistry C, 18*(32), 18299–18306.
145. Unni, K. N. N., Dabos-Seignon, S., Pandey, A. K., & Nunzi, J.-M. (2008). Influence of the polymer dielectric characteristics on the performance of pentacene organic field-effect transistors. *Solid-State Electronics, 52*(2), 179–181.
146. Pierre, A., Gaikwad, A., & Arias, A. C. (2017). Charge-integrating organic heterojunction phototransistors for wide-dynamic-range image sensors. *Nature Photonics, 11*, 193–199.
147. Hwang, I., Kim, J., Lee, M., Lee, M.-W., Kim, H.-J., Kwon, H.-I., Hwang, D. K., Kim, M., Yoon, H., Kim, Y.-H., & Park, S. K. (2017). Wide-spectral/dynamic-range skin-compatible phototransistors enabled by floated heterojunction structures with surface functionalized SWCNTs and amorphous oxide semiconductors. *Nanoscale, 9*, 16711–16721.
148. Li, F., Ma, C., Wang, H., Hu, W., Yu, W., Sheikh, A. D., & Wu, T. (2015). Ambipolar solution-processed hybrid perovskite phototransistors. *Nature Communications, 6*, 8238.
149. Cao, M., Zhang, Y., Yu, Y., & Yao, J. (2018). Improved perovskite phototransistor prepared using multi-step annealing method. In *Proceedings Volume 10529, Organic Photonic Materials and Devices XX; 105290I*.
150. Baeg, K.-J., Binda, M., Natali, D., Caironi, M., & Noh, Y.-Y. (2013). Organic light detectors: Photodiodes and phototransistors. *Advanced Materials, 25*(31), 4267–4295.
151. Qian, C., Qian, C., Sun, J., Kong, L.-A., Gou, G., Zhu, M., Yuan, Y., Huang, H., Gao, Y., & Yang, J. (2017). Organic phototransistors: High-performance organic heterojunction phototransistors based on highly ordered copper phthalocyanine/para-sexiphenyl thin films. *Advanced Functional Materials, 27*(6), 1604933.
152. Milvich, J., Zaki, T., Aghamohammadi, M., Rödel, R., Kraft, U., Klauk, H., & Burghartz, J. N. (2015). Flexible low-voltage organic phototransistors based on air-stable dinaphtho[2,3-b:2′,3′-f]thieno[3,2-b]thiophene (DNTT). *Organic Electronics, 20*, 63–68.
153. Hayter, C. S., Rasmussen, E., & Rooksby, J. H. (2018). Beyond formal university technology transfer: Innovative pathways for knowledge exchange. *The Journal of Technology Transfer*, 1–8.
154. Jessop, P. G., & Reyes, L. M. (2018). GreenCentre Canada: An experimental model for green chemistry commercialization. *Physical Sciences Reviews, 3*(6), 20170189.